

Non-ergodic effects in the Coulomb glass: specific heat

A. Díaz-Sánchez,^{1,2} A. Möbius,¹ M. Ortuño,² A. Neklioudov,¹ and M. Schreiber³

¹*Institut für Festkörper- und Werkstofforschung, D-01171 Dresden, Germany,*

²*Departamento de Física, Universidad de Murcia, E-30071 Murcia, Spain,*

³*Institut für Physik, Technische Universität, D-09107 Chemnitz, Germany*

(November 4, 2018)

We present a numerical method for the investigation of non-ergodic effects in the Coulomb glass. For that, an almost complete set of low-energy many-particle states is obtained by a new algorithm. The dynamics of the sample is mapped to the graph formed by the relevant transitions between these states, that means by transitions with rates larger than the inverse of the duration of the measurement. The formation of isolated clusters in the graph indicates non-ergodicity. We analyze the connectivity of this graph in dependence on temperature, duration of measurement, degree of disorder, and dimensionality, studying how non-ergodicity is reflected in the specific heat.

I. INTRODUCTION

Disordered systems of interacting localized particles have been extensively studied for over two decades. A characteristic feature of these systems is a complex many valley structure of the energy landscape of the state space [1]. Therefore, at sufficiently low temperatures, the system cannot be considered to be in thermodynamic equilibrium: Gibbs ensemble theory of statistical mechanics, which is based on the equivalence of time and ensemble averages, is not applicable. Thus non-ergodic effects are important.

The Coulomb glass [2,3] is a prominent example of such disordered systems. In heavily doped crystalline semiconductors, amorphous semiconductor-metal alloys, and granular metals, it plays an important role as a semiclassical model for systems of localized states. The dynamical behavior of the Coulomb glass has been studied by several groups: Schreiber et al. [4–7], as well as Pérez-Garrido et al. [8,9] determined numerically the transition probabilities between low-energy many-particle states, and studied the eigenvalues of the transition probability matrix. The former group directly diagonalized this matrix, whereas the latter developed a renormalization method to eliminate the transitions with large rates, what considerably simplifies the diagonalization. A broad distribution of relaxation times over several orders of magnitude was found in both cases. It reflects the glassy behavior of this system. Moreover, Wappler et al. [10] used the damage-spreading algorithm to study the temporal evolution of the system, and found evidence for a dynamical phase transition. Yu studied the time development of the Coulomb gap considering a self-consistent equation for the density of states [11]. She too observed that very long time scales are involved.

The main aim of this work is to study numerically non-ergodic effects in the Coulomb glass analyzing the transitions between many-particle states. We apply this procedure to the investigation of such effects in the specific heat. The paper is organized as follows: Section II introduces the Coulomb-glass model. Section III describes how the low-energy many-particle states are obtained numerically. In Sec. IV, we calculate the transition probabilities between these states, and map the dynamical behavior of the Coulomb-glass sample to a graph. The nodes of the graph represent the many-particle states, and the edges the relevant transitions between them. Analyzing the structure of this graph, we determine the value of a physical observable in dependence on the duration of its measurement. In Sec. V, we use this method for the investigation of the non-ergodic effects in the specific heat: We study the influence of temperature, duration of measurement, disorder, and dimensionality. Finally, in Sec. VI we extract some conclusions.

II. MODELS

The classical impurity band (CIB) model is the most realistic model for simulating an impurity band of localized states in a lightly doped semiconductor when quantum interference can be neglected [2,3,12]. It is applicable if the following two conditions are fulfilled: (i) The mean nearest-neighbor distance is considerably larger than the localization radius of the wavefunction of an isolated impurity state. (ii) The temperature is so low that both the activation to the conduction band / from the valence band, and the formation of doubly charged donors / acceptors can be neglected.

We consider a d -dimensional sample of an n -type, partially compensated semiconductor with donor concentration N_D , and acceptor concentration $N_A = KN_D$. The degree of compensation K can range from 0 to 1. So donors are either occupied, that means neutral, or empty, that means positively charged. Acceptors captured an electron each, and are negatively charged. The distribution of electrons between the donors is governed by the Hamiltonian

$$H = - \sum_{i\nu} \frac{1 - n_i}{r_{i\nu}} + \sum_{i < j} \frac{(1 - n_i)(1 - n_j)}{r_{ij}}. \quad (1)$$

The donor occupation number n_i equals 1 for occupied donors, and 0 for ionized donors. Moreover, $r_{i\nu} = |\mathbf{r}_i - \mathbf{r}_\nu|$ and $r_{ij} = |\mathbf{r}_i - \mathbf{r}_j|$, where the random positions of the donors are denoted by \mathbf{r}_i and \mathbf{r}_j , and those of the acceptors by \mathbf{r}_ν . However, to minimize size effects, we impose periodic boundary conditions and use the minimum image convention [13]. That means, in computing $|\mathbf{r}_i - \mathbf{r}_j|$, we substitute the projection of $|\mathbf{r}_i - \mathbf{r}_j|$ onto each of the coordinate axis, $x_i^{(\delta)} - x_j^{(\delta)}$ with $\delta = 1, \dots, d$, by the smallest related value in a periodically repeated representation, $\text{Min}(|x_i^{(\delta)} - x_j^{(\delta)}|, L - |x_i^{(\delta)} - x_j^{(\delta)}|)$ with L being the edge size of the sample. For numerical reasons, we construct the samples so that the nearest neighbor distance exceeds 0.5, a well justified approximation for amorphous semiconductors, but not for crystalline systems. In this work, the unit of distance is defined by the donor density $\rho \equiv 1$, and electron charge, dielectric constant, and Boltzmann constant are taken to be unity.

Within the present study, most of the calculations are performed for a simplified version of this model. Following Refs. [14,15], see also [2,3], we consider a partially filled band of elementary charges (particles) localized on a regular lattice formed by the N_D donor sites. Here, the acceptors are substituted by background charges $-K$ at each of the lattice sites, guaranteeing electro-neutrality on average. The disorder is simulated by a random potential ϵ_i . Its values are uniformly distributed between $-B/2$ and $B/2$. Thus, the influence of the randomness of the donor positions is ignored, as well as the correlations between the values of the acceptor potential at neighboring donor sites. Moreover, the rectangular distribution of the ϵ_i is a simplification neglecting contributions from particular close pairs of donors and acceptors. This model is represented by the Hamiltonian

$$H = \sum_i \epsilon_i n_i + \sum_{i < j} \frac{(n_i - K)(n_j - K)}{r_{ij}}, \quad (2)$$

where $n_i \in \{0, 1\}$ denotes again the occupation number of site i . As above, r_{ij} is the distance between sites i and j according to periodic boundary conditions. The lattice spacing is taken as unit of distance.

A mixed form of both the models (1) and (2) is obtained in the following way: The sites are positioned at random, and the acceptor potential is substituted by a random on-site potential plus the potential of neutralizing charges $-K$ at each site [16,17]. This mixed form is more realistic than Eq. (2): it keeps the donor disorder as the Hamiltonian (1), but simplifies the disorder contribution from the acceptors. By means of ϵ_i , the influence of the random surroundings of host atoms in an amorphous semiconductor can be simulated. This model is in the following referred to as random-position-with-random-potential model.

The relaxation procedures, which we use, alternatively simulate the sample to be isolated, or to be in contact with a particle reservoir [18]. The latter means that, instead of H , the grand canonical potential, $h = H - \mu \sum_i n_i$, is minimized. The value of the chemical potential μ depends on K , i.e., it is fixed by the electro-neutrality condition. Here, we first obtain μ performing a canonical simulation with reduced accuracy. Then we calculate the set of low-energy states, as described below, taking into account particle exchange with the reservoir.

III. DETERMINATION OF A SET OF LOW-ENERGY STATES

For studying low-temperature properties treating correlations exactly, we need to know a set \mathcal{S} of almost all many-particles states in a certain energy interval above the ground state energy. If the occupation numbers are known, the energy of a state can easily and directly be determined from Eq. (1) because we are treating a classical system. The problems, however, consist in the binomially large number of possible configurations, and in the existence of many local minima. Thus it is a complicated task to obtain such a set of low-energy many-particle states. It has been approached by several methods: Mochena and Pollak [19] developed an approximative renormalization-like procedure. Schreiber and Tenelsen [20,21] used the Metropolis algorithm to collect low-lying states which seems to be favorable in comparison to the previous method [22]. Möbius and Pollak [23], and Pérez-Garrido et al. [17] used two-stage algorithms. In the first stage, they obtained sets of local minima by means of relaxation. For that, a complete search considering rearrangements of the site occupations including up to four sites, and an incomplete search concerning

more complex rearrangements, built up of several low-energy one-electron hops (shifts), were performed in Refs. [23] and [17], respectively. In the second stage, both groups completed the table of low-energy states by systematically investigating the neighborhood (in the configuration space) of each of these states. This neighborhood is defined via the accessibility within only one of the considered rearrangements.

Here, we find the set \mathcal{S} of N low-energy many-particle states by means of a three-stage algorithm; for a short preliminary description see Ref. [16]. In the first two stages, we create, and improve a “backbone” of \mathcal{S} , formed by metastable states, the number of which can be considerably smaller than N . Then, in the third stage, we complete \mathcal{S} by systematically investigating the neighborhood of the states found. Our procedure, which includes sophisticated local search [24], and thermal cycling [25], is explained in detail in the following.

In the first stage, creating the backbone of \mathcal{S} , we repeatedly start from states chosen at random, and simulate quenching the sample (i.e., a rapid relaxation) by means of a local search procedure: In an iterative process, we search the neighborhood of the actual state for states of lower energy, and accept always the first such state found. The process stops when no lower neighboring state exists.

Our local search algorithm [24] ensures stability with respect to rearrangements concerning one up to four sites. Making use of the branch-and-bound idea in order to avoid unnecessary attempts to a large extent, it considers the following rearrangements:

- (a) transition of one electron between the sample and a reservoir,
- (b) arbitrary one-electron hops within the sample,
- (c) rearrangements by performing simultaneously an (a) and a (b) transition, and
- (d) arbitrary two-electron hops within the sample.

To ensure high efficiency of the simulations, the searches in (c) and (d) have to be restricted to a certain number of neighbors. For one-, two-, and three-dimensional systems, we consider the first 4, 8, and 26 neighbors, respectively. (Though the number of possible rearrangements increases rapidly with the number of neighbors considered, the portion of long-range hops among the energy decreasing rearrangements is small due to the decreasing interaction strength.)

The second stage consists in extending, and improving this set of metastable states by thermal cycling [25]. For that, a further set \mathcal{M} of metastable states is considered. Initially, it equals a subset of \mathcal{S} , containing the states of lowest energy. We cyclically choose one of the states from \mathcal{M} , and apply to it a Metropolis process with a certain temperature. This process, which is referred to as heating, is terminated, however, after a small number of successful steps. Thus a great part of the information on the ground state, gained within the previous cycles, is retained. Then we quench the sample by means of the above local search algorithm. If the energy of the final state is lower than the energy of the initial state, the latter is substituted in \mathcal{M} .

For each of the final states of these cycles, we check whether or not it is already contained in \mathcal{S} . If not, and if, moreover, the total number of states is smaller than its maximum value, we add it to \mathcal{S} . However, if the final state is not contained within \mathcal{S} , but \mathcal{S} has been already “filled”, we substitute the final state for the state in \mathcal{S} of highest energy, provided the energy of the final state is lower than the energy of the latter.

Several details of thermal cycling should be mentioned: When starting, the temperature of the Metropolis process is chosen to be equal to the total energy gain in quenching a random state divided by the number of sites. In the course of the thermal cycling procedure, this temperature is reduced gradually. The cyclic procedure continues until its efficiency becomes so low that, within a “reasonable” number of cycles, the set \mathcal{M} has not been improved further. In the heating, we consider only two kinds of rearrangements, namely (a) and (b). For $d = 1, 2$, and 3 , the latter are restricted to the first 4, 8, and 26 neighbors, respectively. During this process, we fix the occupation of those sites which have the same n_i value in all states contained in \mathcal{M} because these values obviously favor a low energy. Moreover, in order to diminish the portion of unsuccessful attempts in the Metropolis process, we further reduce the set of rearrangements considered: We tabulate the relevant rearrangements after each temperature change, as well as after adding a new state to \mathcal{M} . As relevance criterion, we use the condition that, for at least one of the states in \mathcal{M} , the related energy change must be smaller than the temperature. In heating, we consider only the excitations stored in this table. Each heating is terminated after having performed 50 rearrangements.

In the third stage, we complete the set \mathcal{S} of low-energy states by systematically investigating the neighborhood (in the configuration space) of the states found [17,23]: For each state in \mathcal{S} , we construct all neighboring states, considering the same types of rearrangements as above. However, we perform (c) and (d) searches (restricted also here to the first 4, 8, and 26 neighboring sites if $d = 1, 2$, and 3 , respectively) only for those states, which are local minima with respect to the (a) and (b) rearrangements. Each new state is added to \mathcal{S} if the number of states in \mathcal{S}

smaller than its maximum value. Otherwise, we substitute the highest-energy state in \mathcal{S} provided the energy of the new state is lower.

This completion procedure starts with the state which has the highest energy, and proceeds cyclically until all states contained in \mathcal{S} have been investigated. If the number of states in \mathcal{S} is large, the decision whether or not the current state has been added to \mathcal{S} already previously, is particularly CPU time consuming. This decision is significantly accelerated by searching hierarchically in an array ordered according to the energies, where pointer arithmetics is used.

To check our program, we performed a series of tests. The degree of completeness of the spectrum of many-particle states within a certain energy interval above the ground state energy was judged in a similar way as in Ref. [23]. We observed that the completeness and the CPU time required do not only depend on the number N of states included in \mathcal{S} , and on the number of local searches performed in the first stage, but to a considerable extent also on the number of states in \mathcal{M} . In the numerical experiments described in Sec. V, N has values between 25 000 and 75 000 what ensures that the width of the related energy interval exceeds the temperature by at least a factor of 25. We found that it is a good choice to adjust the number of local searches in the first stage to $N/25$, and the number of states in \mathcal{M} to $N/500$. Naturally, the kinds of rearrangements considered in the three stages are very important too.

We devoted special attention to testing the thermal cycling part, which improves the backbone of \mathcal{S} . Its efficiency in finding states of particularly low energy is illustrated by Fig. 1. This graph presents the mean energy of the lowest state found in dependence on the CPU time required, contrasting results for simulated annealing (same rearrangements as in heating), sophisticated multi-start local search (repeatedly quenching states chosen at random by means of rearrangements (a) - (d)), and thermal cycling. Fig. 1 shows that, in searching for states of very low energy, thermal cycling is not only far superior to simulated annealing, but also to the sophisticated multi-start local search algorithm. Thus the incorporation of thermal cycling leads to a considerable efficiency increase in the construction of sets of low-energy many-particle states.

As a check of our numerical approach to obtaining almost complete sets of low-energy many-particle states, we verified that the corresponding results for the equilibrium specific heat agree with Refs. [23,26].

IV. INFLUENCE OF THE DURATION OF MEASUREMENT

Our main aim is to study the influence of the duration τ_m of the measurement, during which the state of the sample travels randomly through its configuration space, on the expectation value of an observable O . For that, we decompose the configuration space into separate regions, isolated from each other on the time scale τ_m , in other words, into clusters of states. Two approximations are basic for this approach: (i) The duration of measurement is long enough for establishing thermal equilibrium inside each cluster. (ii) Transitions between different clusters are so rare that they can be ignored on the time scale of the measurement.

First, we calculate the transition probability per unit time from the many-particle state I to the state J . According to Ref. [2], it is given by

$$W_{I \rightarrow J} = w_0 \exp\left(\frac{-2 \sum r_{ij}}{a}\right) \begin{cases} \exp[(E_I - E_J)/T] & \text{if } E_I < E_J \\ 1 & \text{if } E_I > E_J \end{cases} \quad (3)$$

In this equation, the parameter w_0 is a constant of the order of the phonon frequency, $w_0 \sim 10^{13} \text{ s}^{-1}$. a denotes the localization radius, and E_I the energy of the state I . The sum term is an abbreviation of the minimized sum of the related hopping lengths; it concerns only those sites, the occupation of which is changed in the transition. That means, we decompose the many-electron transition into independent one-electron hops. Among all possible such decompositions, we choose that for which the sum of the lengths of the one-electron hops takes its minimum value.

Presuming the occupation probabilities of the states to have their thermodynamic equilibrium values, we obtain the rate of transitions from state I to state J ,

$$R_{I \rightarrow J} = W_{I \rightarrow J} \exp\left(\frac{-E_I}{T}\right) Z^{-1} \quad (4)$$

where Z is the partition function. In thermodynamic equilibrium, $R_{I \rightarrow J} = R_{J \rightarrow I}$. Thus the transition time, i.e., the inverse of the equilibrium transition rate, is given by

$$\tau_{IJ} = \tau_0 \exp\left(\frac{2 \sum r_{ij}}{a} + \frac{E_{IJ}}{T}\right) Z \quad (5)$$

with $E_{IJ} = \max(E_I, E_J)$, and $\tau_0 = w_0^{-1}$.

Now, we map the dynamics of the Coulomb glass sample simulated to a graph, where the nodes represent the states, and the edges those transitions between them for which $\tau_{IJ} < \tau_m$. The nodes which are directly or indirectly connected with each other by such edges form clusters. These clusters correspond to regions of the configuration space being isolated from each other on the time scale τ_m . Here we presume equilibrium in determining τ_{IJ} . However, this principle can easily be generalized to the non-equilibrium case, see below.

Provided, at the beginning of the measuring process, the sample is in one of the states of the cluster α , we measure as value of the observable O ,

$$\langle O \rangle_\alpha(T) = \sum_{I \in \alpha} O_I \exp\left(\frac{-E_I}{T}\right) Z_\alpha^{-1}, \quad (6)$$

where O_I denotes the value of O for the state I , and Z_α the partition function of this cluster. The values of $\langle O \rangle_\alpha$ can have a very broad distribution.

Finally, we turn to the expectation value of O , that is the mean value of repeated measurements, referred to in the following as $\langle\langle O \rangle\rangle(T, \tau_m)$. The probability to find the sample in one of the states belonging to the cluster α be P_α . Thus, $\langle\langle O \rangle\rangle$ is given by the weighted average of the $\langle O \rangle_\alpha$:

$$\langle\langle O \rangle\rangle(T, \tau_m) = \sum_{\alpha} \langle O \rangle_\alpha P_\alpha. \quad (7)$$

In consequence, $\langle\langle O \rangle\rangle$ depends via the cluster structure and P_α on τ_m , and also on T .

Both the cluster structure and P_α are influenced by the history of the sample. In our numerical experiments, we have simulated two situations:

- (A) As standard case, we presume that the sample has reached thermal equilibrium before the measurements; thus $P_\alpha = Z_\alpha/Z$.
- (B) Alternatively, we assume the sample to have been quenched from infinite T to the measuring T within a short time interval τ_q . To emulate this process we quench first to $T = 0$, and heat then immediately to the measuring T : In the beginning, we assign the same probability to all states, $P_I = 1/N$. Then, we perform the following iteration treating the states according to decreasing energy. We re-distribute the weight of the considered state to all those states of lower energy to which a transition can happen within τ_q modifying the set of the P_I correspondingly. The related transition times are obtained in a way analogous to the derivation of Eq. (5). That means, substituting the equilibrium occupation probabilities by the (iteration cycle dependent) non-equilibrium P_I , we get for the transition $I \rightarrow J$

$$\tau_{I \rightarrow J} = \begin{cases} \infty & \text{if } E_I < E_J \\ w_0^{-1} \exp(2 \sum r_{ij}/a) P_I^{-1} & \text{if } E_I > E_J \end{cases}. \quad (8)$$

Thus the quenching process is related to the modification of parts of the states graph (differing from the “equilibrium graph”) in each of the iteration steps. At the end of the iteration, only the local minima have a finite occupation probability. Finally, we assign to each “equilibrium cluster” the sum of the occupation probabilities of the included “non-equilibrium local minima”. In this way, we calculate the non-equilibrium values of P_α , but we neglect the influence of the preparation mode on τ_{IJ} , and thus on the structure of the clusters which are isolated from each other on the time scale τ_m .

V. NON-ERGODIC SPECIFIC HEAT

Applying the methods presented in Secs. III and IV to the study of non-ergodic effects in the specific heat, we start from the definition of this observable for a cluster α of states, which is in thermal equilibrium:

$$c_\alpha(T) = \frac{\langle H^2 \rangle_\alpha - \langle H \rangle_\alpha^2}{T^2 N_D}. \quad (9)$$

Since the specific heat is by itself a quantity relating to an ensemble of states rather than to a single state, we do not need brackets here to mark the averaging over the states in the cluster α , in deviation from the general notation

$\langle O \rangle_\alpha(T)$ in Eq. (6). After averaging over the set of clusters, the τ_m dependent value of the specific heat $\langle c \rangle(T, \tau_m)$ is obtained utilizing Eq. (7).

To make the influence of τ_m directly visible, we consider the quotient of the values of the specific heat for finite and infinite duration of measurement, respectively:

$$q(T, \tau_m) = \frac{\langle c \rangle(T, \tau_m)}{\langle c \rangle(T, \infty)}. \quad (10)$$

This quantity is in the following referred to as non-ergodicity quotient. Studying $q(T, \tau_m)$ rather than $\langle c \rangle(T, \tau_m)$ is additionally motivated by numerical reasons: The random fluctuations of q from sample to sample are considerably smaller than the fluctuations of $\langle c \rangle$. Moreover, in order to characterize the fluctuations of c from measurement to measurement, we consider its root-mean-square deviation, related to the distribution of the clusters,

$$\sigma^2(T, \tau_m) = \sum_\alpha P_\alpha \left(\frac{c_\alpha(T, \tau_m) - \langle c \rangle(T, \tau_m)}{\langle c \rangle(T, \infty)} \right)^2. \quad (11)$$

Investigating the physical properties of macroscopic systems, we have calculated ensemble averages, and have compared the results for different sample sizes. The number of samples to be taken into account depends not only on the accuracy to be achieved, but also on all the various details of the simulated situation. Generally, we have chosen the size of the samples so large that corresponding convergence of the results is ensured. The related parameter values are given in the figure captions.

Several details of our simulations have to be mentioned: The localization radius a equals always 0.2 [27]. Decreasing its value corresponds, crudely speaking, to stretching the time scale, and thus enhances the non-ergodic effects. Since a great part of the literature concerns the simplified Coulomb glass model according to Eq. (2) (sites arranged on a regular lattice), we, too, consider this situation in most of the simulations. Thus, if not stated otherwise, our numerical experiments have been performed for this model. The results presented here have been obtained by means of a canonical procedure: In calculating $\langle c \rangle$, we take into account only the low-energy states with total charge equal to KN_D . When the grand canonical procedure is used for this aim, finite-size effects are more important since, due to differing total charge, some clusters remain separated from each other in configuration space even if $\tau_m \rightarrow \infty$.

In the following, we discuss our numerical results in detail. First, we consider the non-ergodicity quotient q . As examples, Figs. 2a and 2b illustrate for three-dimensional samples with two different degrees of disorder, how finite-size effects influence the dependence of q on the duration of measurement τ_m . They show that finite-size effects are particularly important for large τ_m , where extended clusters of states have to be considered. However, if the sample size N_D exceeds a certain value, roughly 500 for the cases considered here, q is almost independent of N_D . Certainly, this limit depends on the concrete situation considered, i.e., on T , B , and d , and also on τ_m .

Moreover, Fig. 2 leads to an important conclusion: The value of τ_m where q reaches (almost) 1 can be interpreted as relaxation time of the specific heat. It exceeds typical experimental times by several orders of magnitude. This indicates glassy behavior, where non-ergodic effects are fundamental.

In Fig. 3, we show $q(\tau_m)$ and its fluctuation σ defined by Eq. (11). These data illustrate that the measured values of c are distributed within a wide range around the mean value, what originates from the varying properties of the separated clusters of states. This is a manifestation of the non-ergodic effects. However, for drawing further conclusions, a detailed study of the size dependence of σ would be needed.

Figure 4 displays the temperature dependence of the specific heat for two values of τ_m , as well as for thermal equilibrium (infinite τ_m). Moreover, this figure compares the changes caused by variation of T with the influence of τ_m .

Now we study the non-ergodicity quotient q in more detail. Fig. 5 illustrates that the strength B of the disorder has only a weak influence within the considered parameter range. Only for $B = 1$, a small systematic shift of $q(\tau_m)$ towards higher τ_m is detectable in comparison to the curves for stronger disorder. If τ_m is so large that q reaches almost 1, decreasing the disorder enhances the relevance of long-time correlations.

The influence of the temperature T on q is considered in Fig. 6. For τ_m/τ_0 exceeding 10^{10} , we observe the expected behavior, namely that decreasing T is related to the increasing influence of non-ergodicity effects. However, we found a point, $\tau_m/\tau_0 \sim 10^{10}$, where q is almost independent of T within the T region studied. For smaller τ_m , there is even some increase of q with decreasing T . Presumably, the reason of this feature is the following. Decreasing T influences the cluster structure in two ways. On the one hand, it causes a division of clusters due to the decrease of transition rates, and thus an increase of the cluster number. On the other hand, however, the number of really relevant clusters decreases due to the decreasing occupation probability of excited states. We suppose that the second effect is

dominating for small τ_m . There is some analogy to uncorrelated hopping conductivity, which increases exponentially with T in the limit $\omega \rightarrow 0$, but decreases as $1/T$ at high frequency [28]. A similar behavior has also been found in the frequency dependence of the dielectric susceptibility [29].

The question to which extent the obtained results are model dependent is answered in Fig. 7. For the chosen disorder strength, the results for the CIB model and the random-position-with-random-potential model are almost identical. For the lattice model, however, the $q(\tau_m)$ curve is a bit steeper, but the relaxation time of the specific heat is roughly the same as for the other models. Thus, in the region of low q , its $q(\tau_m)$ curve is shifted towards higher τ_m . This effect probably originates from the missing of “easy” hops between closely neighboring sites. Thus the influence of the spatial disorder of the donor sites is clearly stronger than the influence of the details of the random on-site potential ϵ_i . (In the CIB model the acceptors create a potential which is almost Gaussian with a width of 2.5.)

We have also studied the non-ergodicity quotient q for one- and two-dimensional samples. The results, presented in Fig. 8, are similar to the above findings for the three-dimensional case. However, there is a clear trend of non-ergodicity effects becoming more and more pronounced with decreasing dimension in the region of large τ_m . Thus the reduction of the dimension seems to be related to a stronger “localization” of the particles.

Finally, we consider the question how the sample preparation influences $q(\tau_m)$. Fig. 9 shows results for the lattice model. Here, we compare samples being in thermal equilibrium with samples prepared by quenching. The latter curve is shifted towards larger τ_m . However, this effect decreases with increasing B , compare with Fig. 2 in [16]. Thus it is natural that the preparation conditions have a weaker influence for the other two Coulomb glass models considered.

VI. CONCLUSIONS

In the previous sections, we have presented a numerical algorithm for studying the non-ergodic effects in the Coulomb glass, which are very important at low temperatures. This method considers many-particle states, and takes into account correlations completely. Here, it has been used for investigating how the mean value of the specific heat $\langle c \rangle$ depends on the measuring time. The main results of our numerical experiments are summarized in the following points:

- (i) The non-ergodicity quotient $q(T, \tau_m) = \langle c(T, \tau_m) \rangle / \langle c(T, \infty) \rangle$ strongly depends on the measuring time τ_m . It vanishes as $\tau_m \rightarrow 0$, and, in the cases studied here, it approaches 1 only for values of τ_m which exceed realistic measuring times by orders of magnitude.
- (ii) For large τ_m , q decreases with decreasing T , whereas an increase of q with decreasing T is observed in the region of small τ_m .
- (iii) Spatial disorder has a larger influence on the non-ergodic effects than the strength of the on-site random potential in the lattice model.
- (iv) The importance of non-ergodic effects increases with decreasing dimensionality.
- (v) Preparing the sample by a quench causes an increase of non-ergodic effects in the case of weak disorder.

Finally, we would like to stress one technical aspect of the simulations. We have improved our previously developed algorithm for the construction of almost complete sets of low-energy many-particle states [23] by adding a thermal cycling [25] part. This method, originally applied to the traveling salesman problem, combines ideas from Monte Carlo and local search algorithms. Here, we have used it when searching for deep local minima in the configuration space of the Coulomb glass. Also in this case, thermal cycling has been proved to be highly efficient.

ACKNOWLEDGMENTS

This work was supported by the SMWK and DFG (SFB 393). A great part of it was performed during A. D.-S.’s visit at the IFW Dresden; A. D.-S. thanks the IFW for its hospitality. We are indebted to M. Pollak for stimulating discussions.

- [1] See, e.g., *Spin Glass Theory and Beyond*, edited by M. Mézard, G. Parisi, and M. Virasoro (World Scientific, Singapore, 1987).
- [2] M. Pollak and M. Ortuño, in *Electron-Electron Interactions in Disordered Systems*, edited by A.L. Efros and M. Pollak (North-Holland, Amsterdam, 1985), p. 287.
- [3] B.I. Shklovskii and A.L. Efros, *Electronic Properties of Doped Semiconductors* (Springer, Berlin, 1984).
- [4] M. Schreiber and K. Tenelsen, *Model. Simul. Mater. Sci. Eng.* **2**, 1047 (1994).
- [5] M. Schreiber and K. Tenelsen, *J. Lumin.* **58**, 130 (1994).
- [6] M. Schreiber and K. Tenelsen, *J. Non-Cryst. Sol.* **172–174**, 457 (1994).
- [7] M. Schreiber, K. Tenelsen, and T. Vojta, *J. Lumin.* **66**, 521 (1996).
- [8] A. Pérez-Garrido, M. Ortuño, and A. Díaz-Sánchez, *phys. stat. sol. (b)* **205**, 31 (1998).
- [9] A. Pérez-Garrido, M. Ortuño, A. Díaz-Sánchez, and E Cuevas. *Phys. Rev. B* **59**, 5328 (1999).
- [10] T. Wappler, T. Vojta, and M. Schreiber, *Phys. Rev. B* **55**, 6272 (1997).
- [11] C.C. Yu, *Phys. Rev. Lett.* **82**, 4074 (1999).
- [12] A.L. Efros and B.I. Shklovskii in *Electron-Electron Interactions in Disordered Systems*, edited by A.L. Efros and M. Pollak (North-Holland, Amsterdam, 1985), p. 409.
- [13] N. Metropolis, A.W. Rosenbluth, M.N. Rosenbluth, A.H. Teller, and E. Teller, *J. Chem. Phys.* **21**, 1087 (1953).
- [14] D. Baranovskii, A.L. Efros, B.I. Gelmont, and B.I. Shklovskii, *J. Phys. C* **12**, 1023 (1979).
- [15] J.H. Davies, P.A. Lee, and T.M. Rice, *Phys. Rev. B* **29**, 4260 (1984).
- [16] A. Díaz-Sánchez, A. Möbius, M. Ortuño, A. Pérez-Garrido, and M. Schreiber, *phys. stat. sol. (b)* **205**, 17 (1998).
- [17] A. Pérez-Garrido, M. Ortuño, E. Cuevas, J. Ruiz, and M. Pollak, *Phys. Rev. B* **55**, R8630 (1997).
- [18] A. Möbius and M. Richter, *J. Phys. C* **20**, 539 (1987).
- [19] M. Mochena and M. Pollak, *Phys. Rev. Lett.* **67**, 109 (1991).
- [20] M. Schreiber and K. Tenelsen, *Europhys. Lett.* **21**, 697 (1993).
- [21] K. Tenelsen and M. Schreiber, *Phys. Rev. B* **49**, 12662 (1994).
- [22] J. Talamantes and D. Esperciceta, *Model. Simul. Mater. Sci. Eng.* **1**, 761 (1993).
- [23] A. Möbius and M. Pollak, *Phys. Rev. B* **53**, 16197 (1996).
- [24] A. Möbius, M. Richter, and B. Drittlér, *Phys. Rev. B* **45**, 11568 (1992).
- [25] A. Möbius, A. Nekliudov, A. Díaz-Sánchez, K.H. Hoffmann, A. Fachat, and M. Schreiber, *Phys. Rev. Lett.* **79**, 4297 (1997).
- [26] A. Möbius and P. Thomas, *Phys. Rev. B* **55**, 7460 (1997).
- [27] M. Mochena and M. Pollak, *J. Non-Cryst. Solids* **131-133**, 1260 (1991).
- [28] M. Pollak, *Phil. Mag.* **23**, 519 (1971).
- [29] A. Díaz-Sánchez, M. Ortuño, M. Pollak, A. Pérez-Garrido, and A. Möbius. *Phys. Rev. B* **59**, 910 (1999).

FIG. 1. Relation between CPU time, τ_{CPU} (in seconds), and mean deviation of the energy of the lowest state found from the ground state energy, $\delta E = E_{\text{mean}} - E_{\text{ground state}}$, for one realization of the three-dimensional lattice model with $B = 1$ and $N_{\text{D}} = 1000$. \times : simulated annealing; \triangle : sophisticated multi-start local search; \bullet : thermal cycling. The values of τ_{CPU} relate to one 180 MHz PA8000 processor of an HP K460. For simulated annealing and multi-start local search, averages were taken from 20 runs, for thermal cycling from 100 runs. In thermal cycling, the ground state was always found within 500 seconds. Error bars (1σ region) are presented if they are larger than the symbols. The interpolating lines are guides to the eye only.

FIG. 2. Influence of the sample size N_{D} on the dependence of the non-ergodicity quotient q on the duration of the measurement τ_m for the three-dimensional lattice model. (a) $B = 1$, $T = 0.006$; (b) $B = 4$, $T = 0.008$. \circ , $+$, and \bullet correspond to $N_{\text{D}} = 216$, 512, and 1000, respectively. The ensemble averaging took into account 200 samples in each case, except for the two curves for $N_{\text{D}} = 512$ and 1000 in (a), where we considered 100 and 50 samples, respectively. The error bars are smaller than the symbol size.

FIG. 3. Fluctuation of the contributions to q from the individual clusters, represented by error bars displaying σ defined by Eq. (11). $B = 1$, $T = 0.008$, and $N_{\text{D}} = 512$. Ensemble averaging took into account 100 samples.

FIG. 4. Temperature dependence of the mean specific heat for thermal equilibrium (\circ), and for two finite measuring times: $\tau_m/\tau_0 = 10^{15}$ (\blacktriangle) and $\tau_m/\tau_0 = 10^{12}$ (\times). The error bars represent the width of the distribution of c_{α} . $d = 3$, $B = 1$ and $N_{\text{D}} = 512$. Ensemble averaging took into account 100 samples.

FIG. 5. Influence of the disorder strength B on $q(\tau_m)$ for the lattice model: \bullet : $B = 1$; $+$: $B = 2$; \circ : $B = 4$. For all curves, $d = 3$, $N_{\text{D}} = 512$, $T = 0.008$. Ensemble averaging took into account 200 samples for $B = 2$ and $B = 4$, and 100 samples for $B = 1$.

FIG. 6. Influence of the temperature T on $q(\tau_m)$ for the lattice model: \bullet : $T = 0.006$; \blacktriangle : $T = 0.008$; $+$: $T = 0.010$; \circ : $T = 0.012$. For all curves: $d = 3$, $B = 1$, and $N_{\text{D}} = 512$; ensemble averaging took into account 100 samples.

FIG. 7. Comparison of the $q(\tau_m)$ obtained for the three different versions of the Coulomb glass model introduced in Sec. II: $+$, \circ , and \bullet denote lattice, CIB, and random-position-with-random-potential models, respectively. For the first and the last model, $B = 2$. In all cases, $d = 3$, $T = 0.008$, and $N_{\text{D}} = 512$; ensemble averaging took into account 200 samples.

FIG. 8. Comparison of the $q(\tau_m)$ obtained for lattice models of different dimensions: \circ : $d = 1$, $N_{\text{D}} = 50$; $+$: $d = 2$, $N_{\text{D}} = 484$; \bullet : $d = 3$, $N_{\text{D}} = 512$. In all cases, $B = 1$, and $T = 0.01$. Ensemble averaging took into account 200 samples for $d = 1$ as well as for $d = 2$, and 100 samples for $d = 3$.

FIG. 9. Influence of sample preparation on $q(\tau_m)$ for the three-dimensional lattice model: \circ : sample in thermal equilibrium; \bullet : sample quenched within $\tau_q = 10^{13} \tau_0 \sim 1$ s. For both curves: $B = 1$, $T = 0.01$, and $N_{\text{D}} = 512$; ensemble averaging took into account 100 samples.

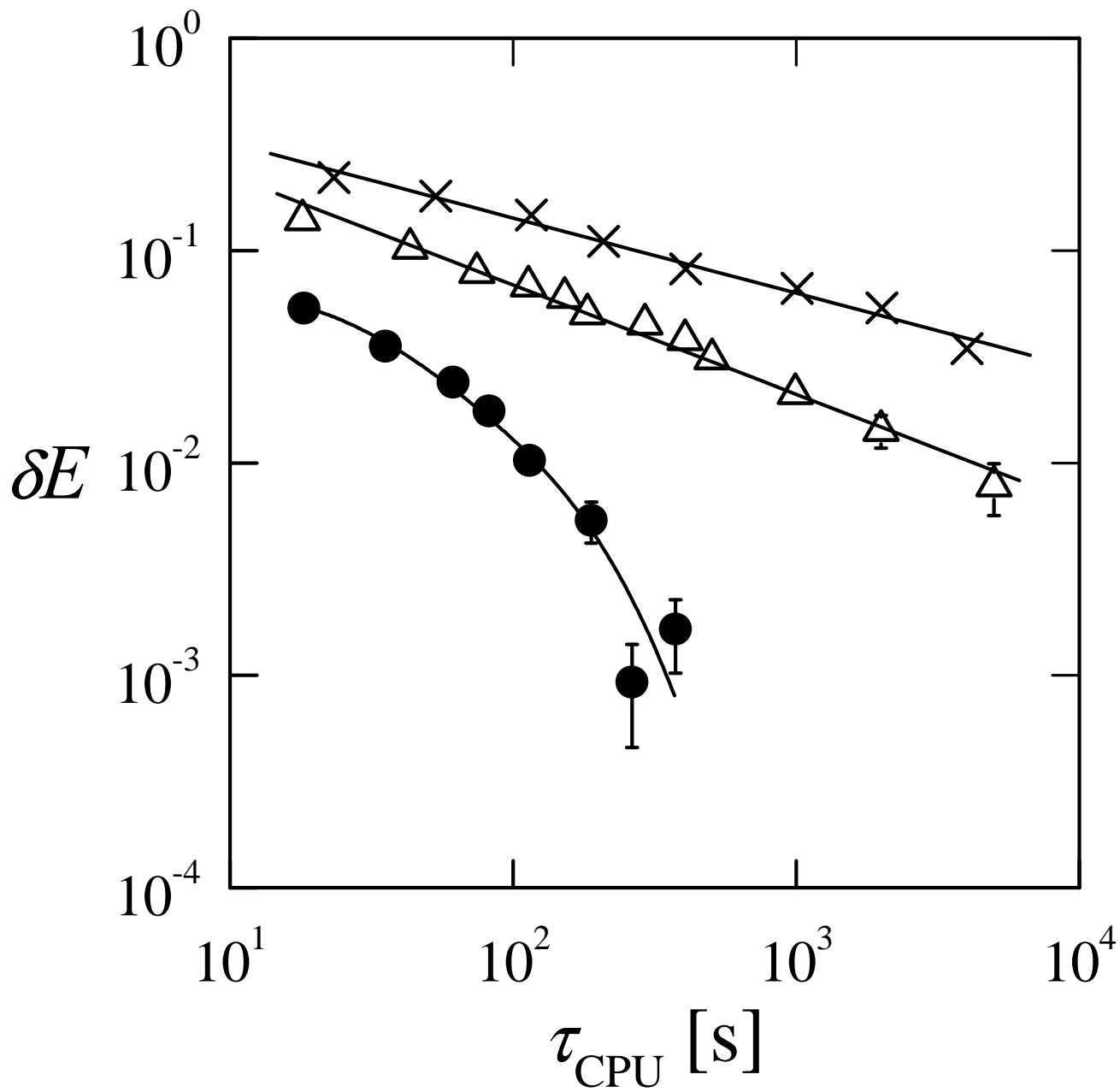


Fig. 1

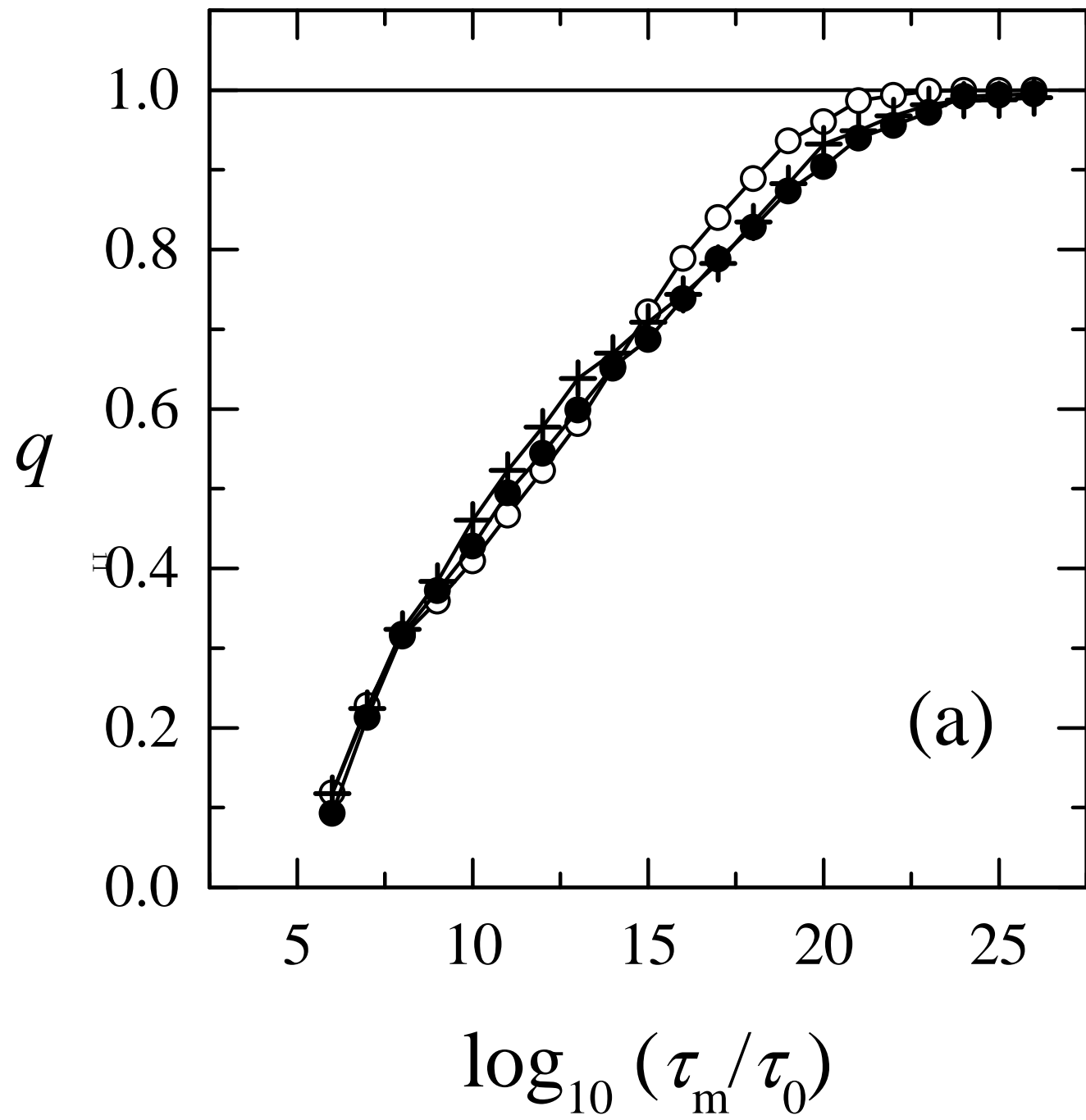


Fig. 2 (a)

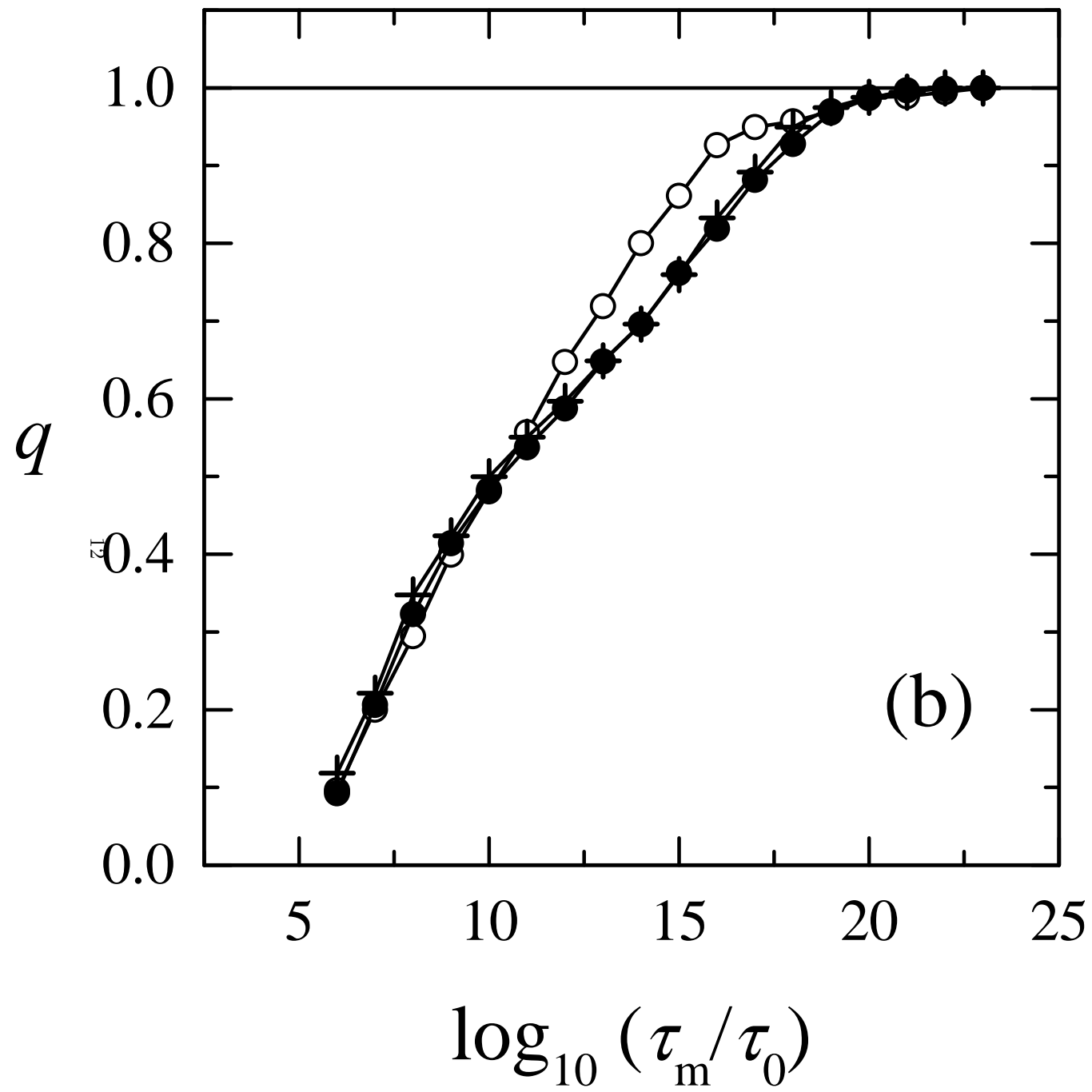


Fig. 2 (b)

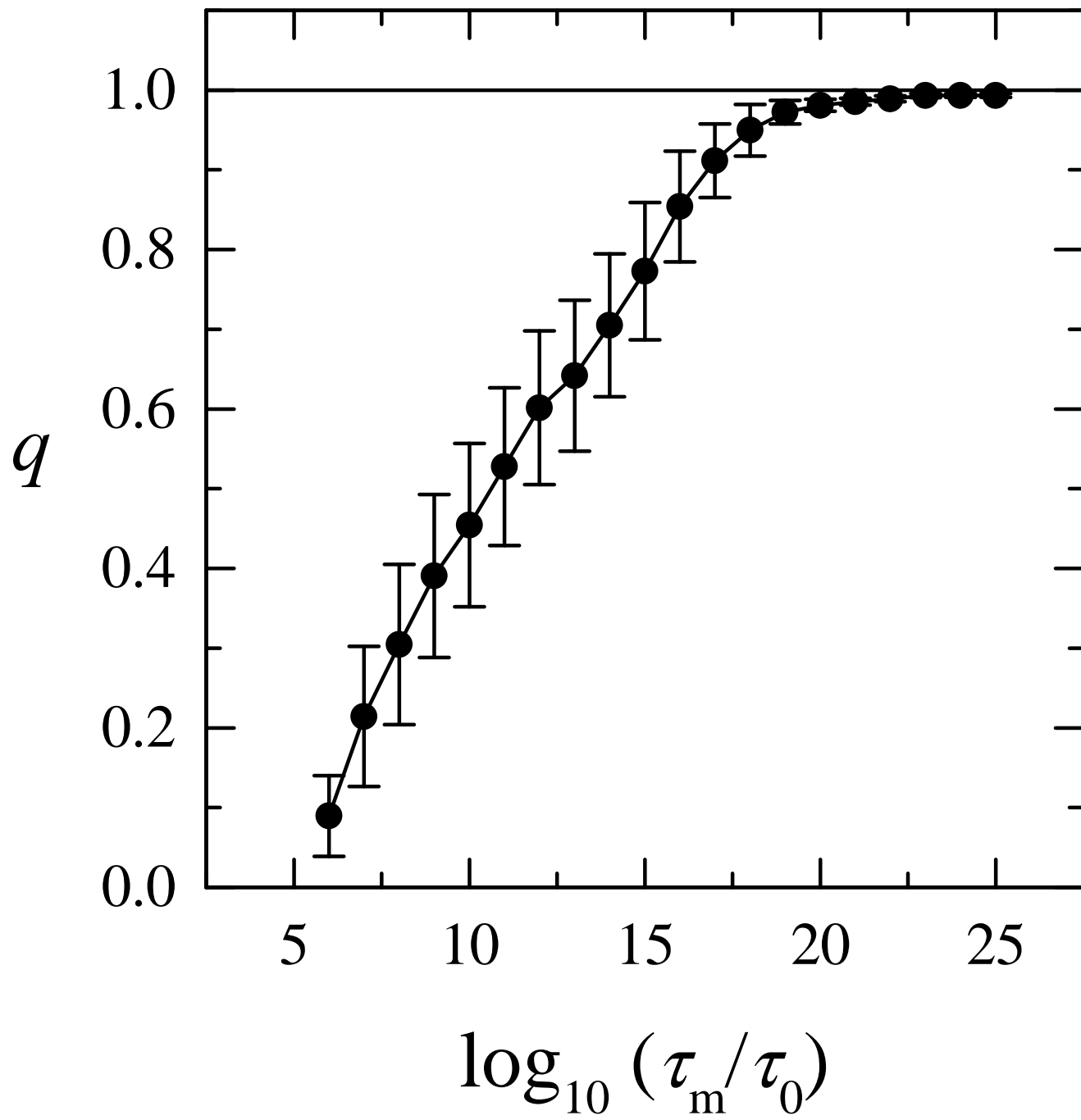


Fig. 3

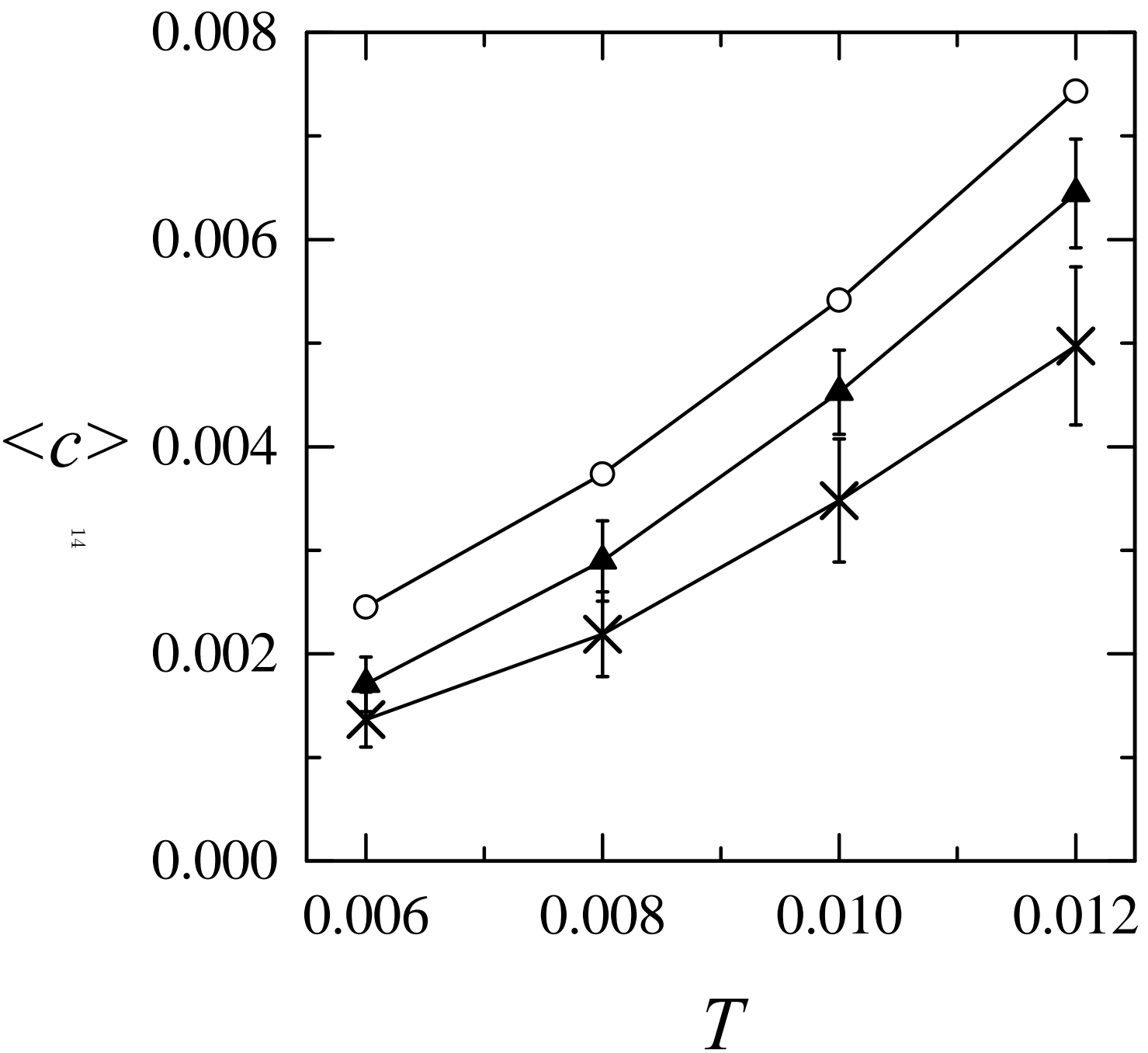


Fig. 4

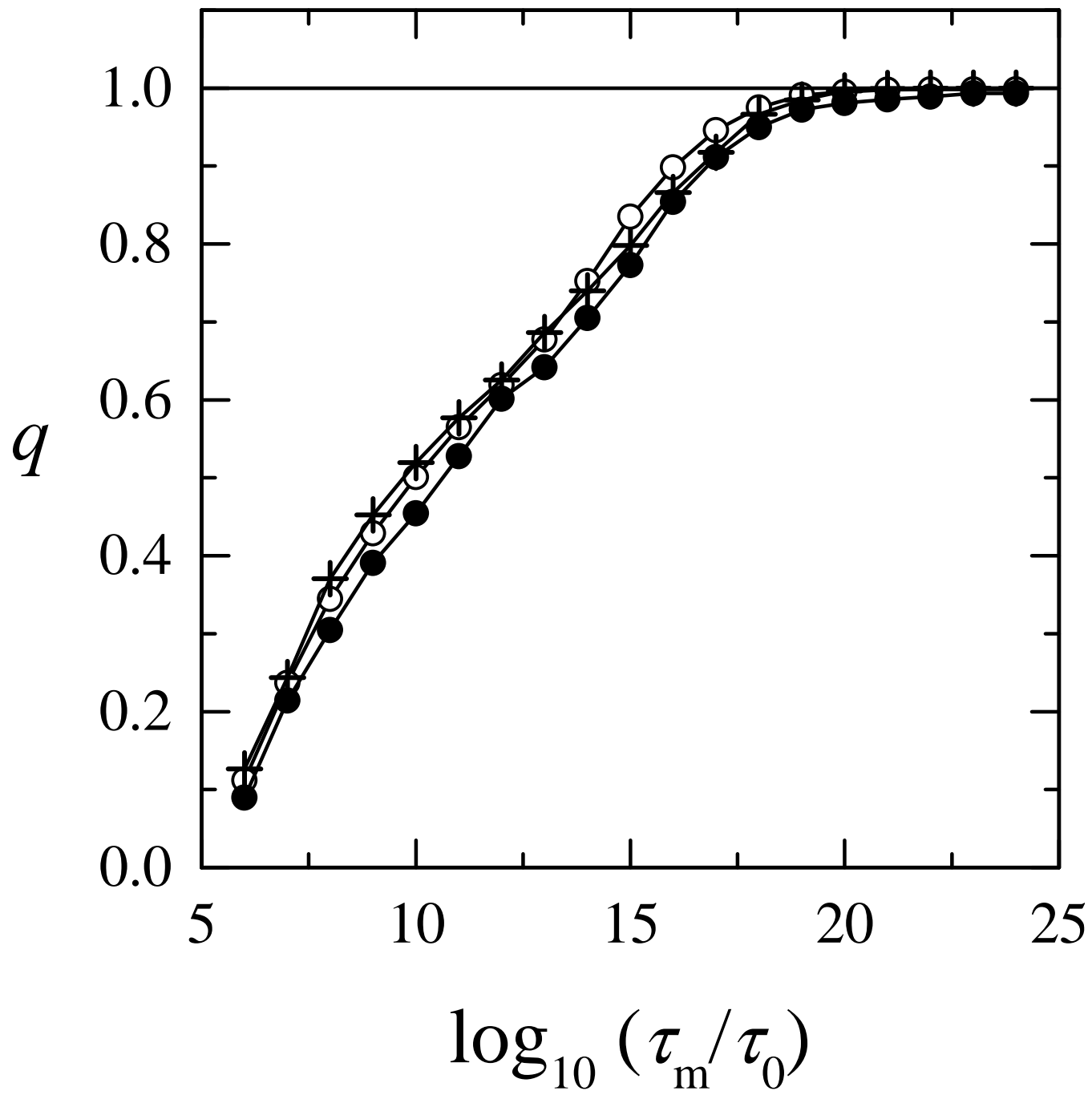


Fig. 5

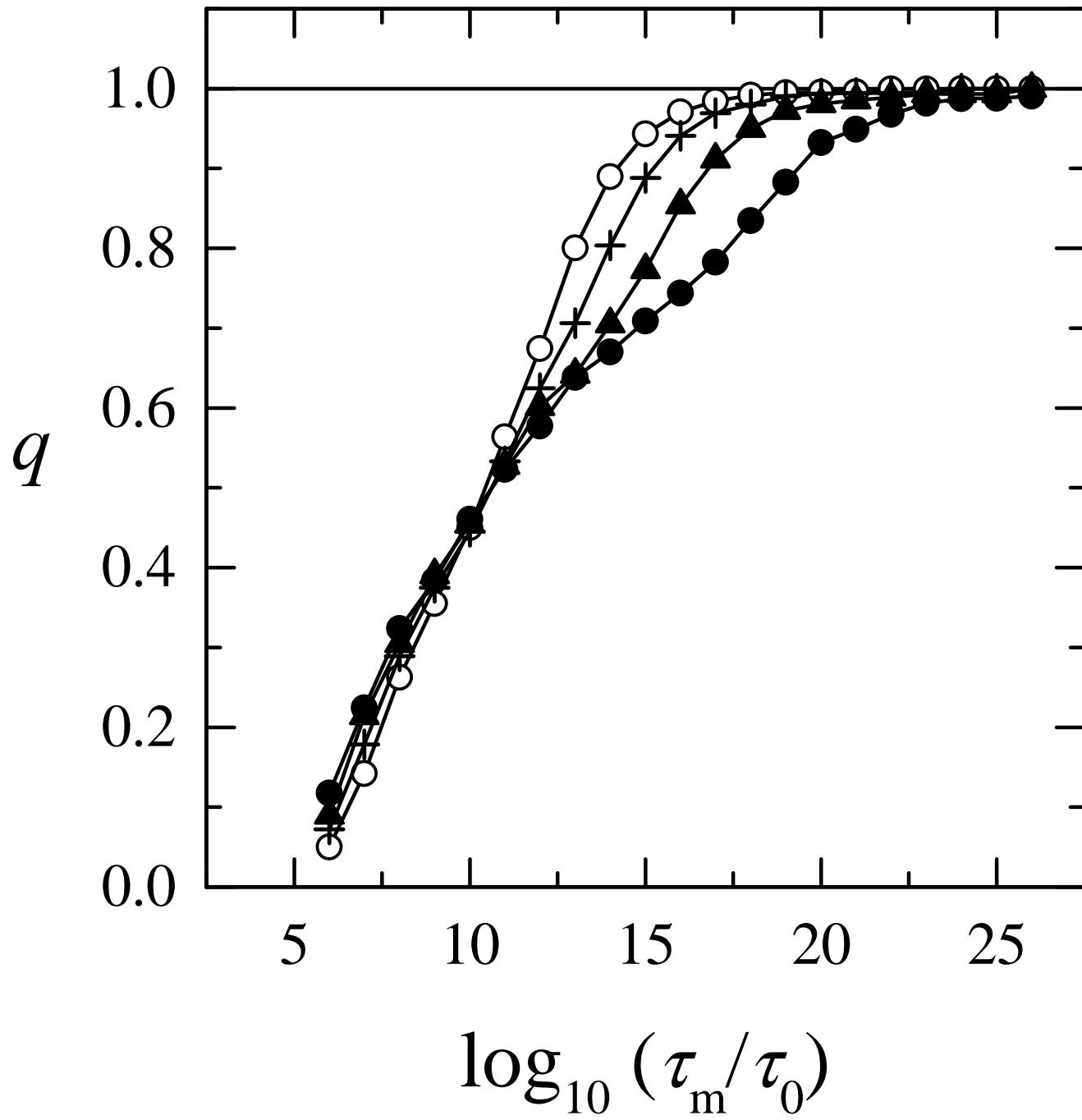


Fig. 6

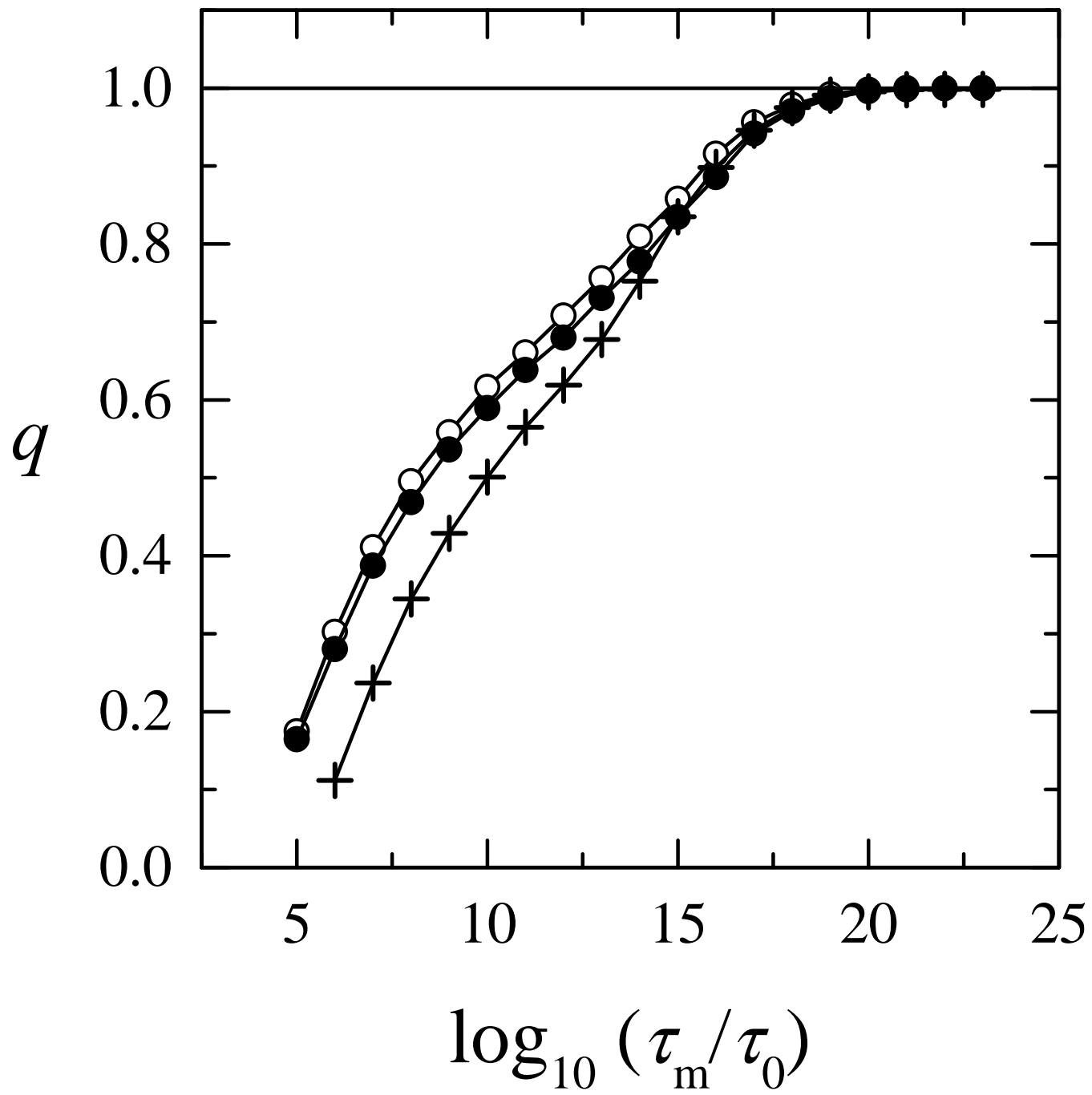


Fig. 7

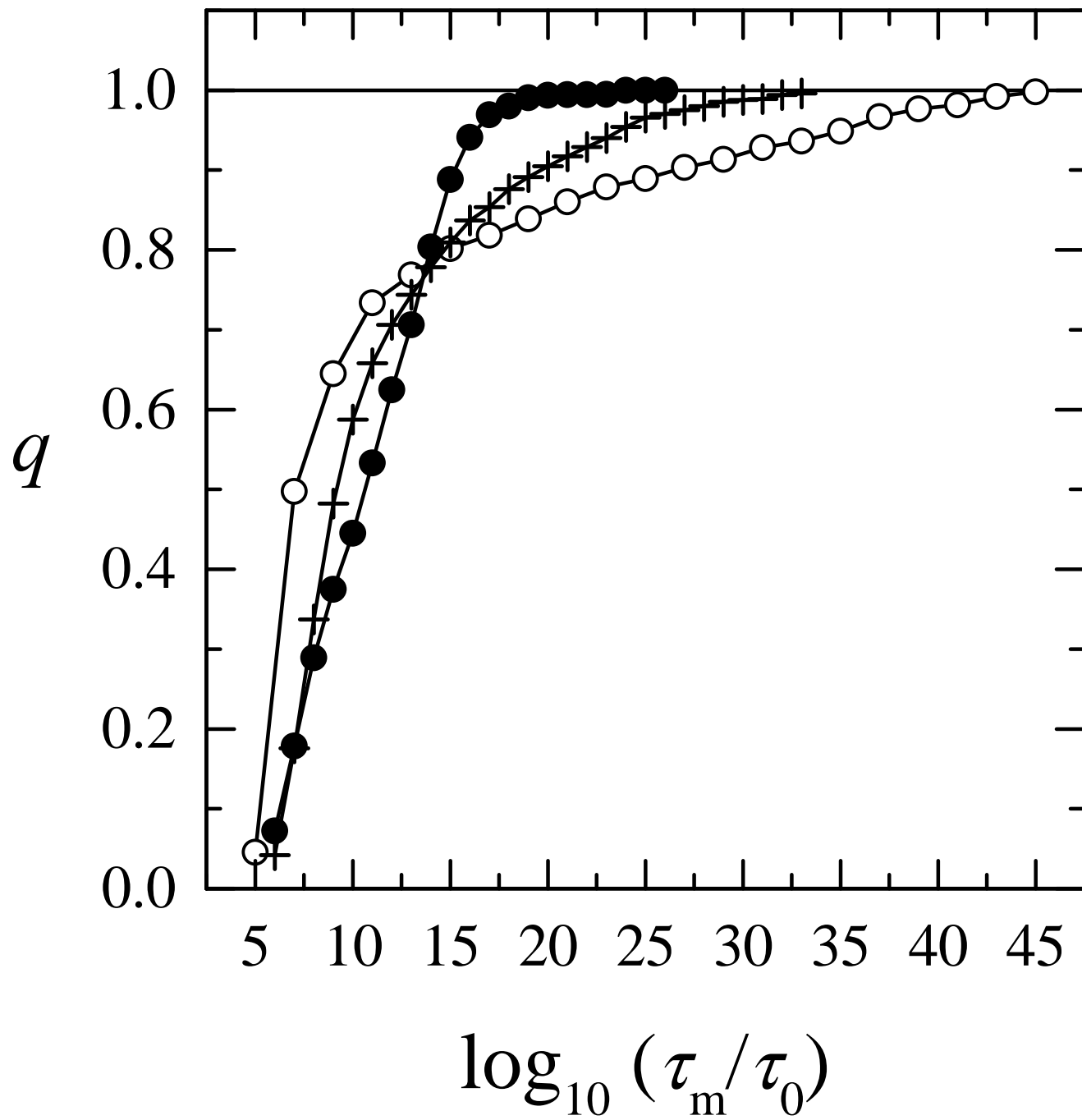


Fig. 8

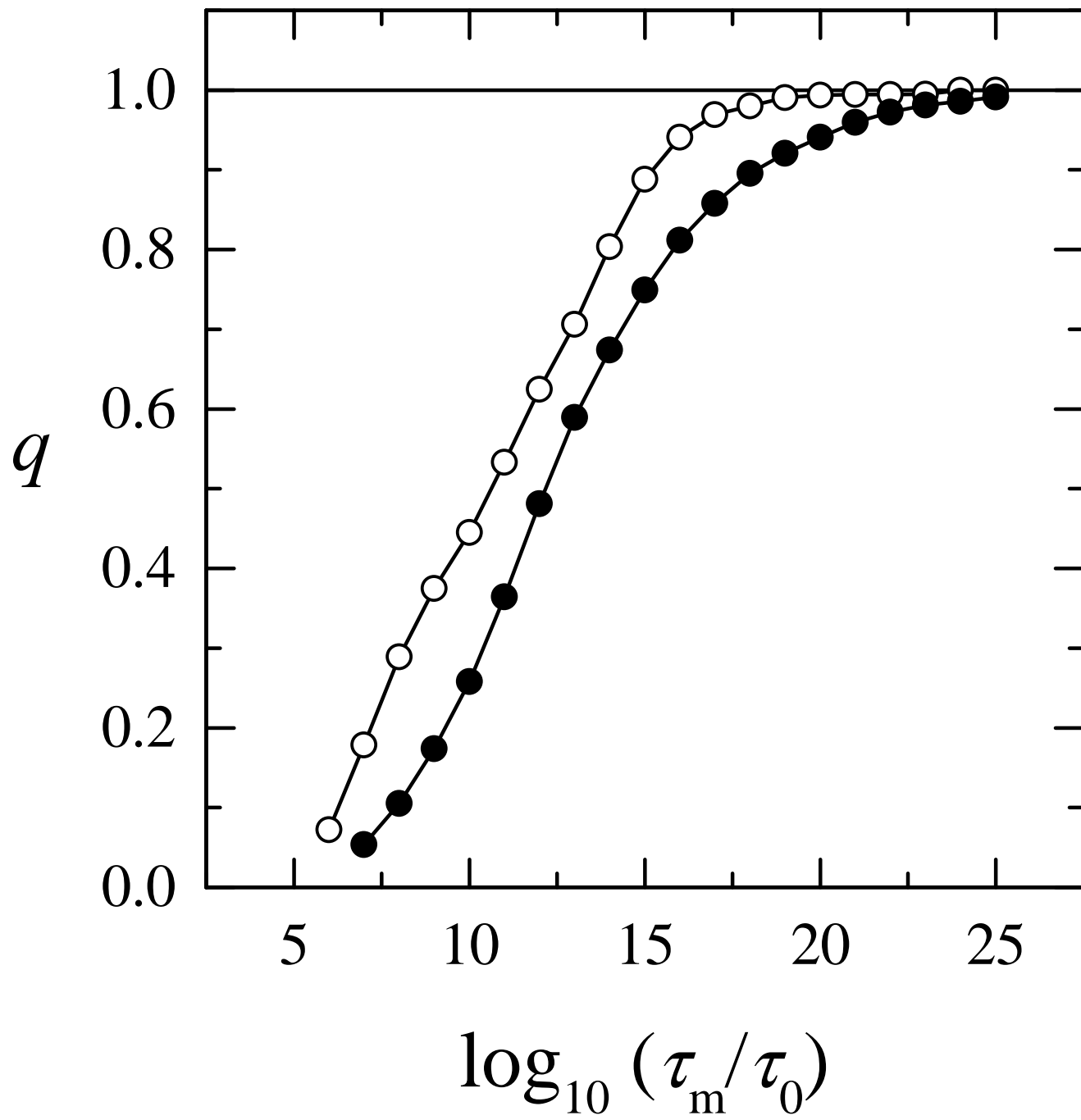


Fig. 9